INTERFACE CURRENT INTEGRAL TRANSPORT METHODS FOR THE CALCULATION OF NEUTRAL ATOM TRANSPORT IN THE EDGE REGION OF FUSION PLASMAS

PLASMA ENGINEERING

KEYWORDS: *neutral transport, edge plasma*

WESTON M. STACEY,* JOHN MANDREKAS, and ROBERT RUBILAR
Georgia Institute of Technology, Nuclear Engineering Program
Atlanta, Georgia 30332-0225

Received May 15, 2000
Accepted for Publication November 4, 2000

Neutral atom transport in the edge region of fusion plasmas is characterized by extreme geometrical complexity, mean-free-paths that vary from millimetres to metres over short distances, and many orders of magnitude variation in atom density. We have proposed and are developing an interface current integral transport method as a more practical alternative to the Monte Carlo method, which is currently used for such calculations. This particular formulation of interface current methodology is described, the accuracy of the several approximations that are made in implementing the methodology are evaluated by comparison with Monte Carlo, and correction factors and extensions of the methodology, which improve accuracy, are presented. The results are formulated so as to be generally applicable to any neutral particle transport application.

I. INTRODUCTION

The neutral atom transport problem in the edge region of a fusion plasma is characterized by geometrically complex regions varying in mean-free-paths (mfp's) from millimetres to metres and by the importance of having accurate results over many orders of magnitude attenuation in neutral atom density. A two-dimensional model of a representative experimental configuration is shown in Fig. 1. Plasma ions escape the central plasma confinement region into a thin "scrape-off layer," where they are swept downward along magnetic field lines to impinge with sonic speed on "divertor plates." These ions are reflected as neutral atoms or reemitted as neutral molecules, which dissociate immediately to form neutral atoms. Most of these neutral atoms interact with the relatively high-density plasma just in front of the divertor plates as they diffuse upstream against the sonic plasma stream flowing to the plates (e.g., in regions 43, 42, 40, 38, etc.). However, some of the neutral atoms escape the dense plasma stream into the very low plasma density regions (e.g., 41, 39, 44, 45, etc.), where they travel relatively unimpeded to the other plasma stream flowing to the other divertor plate, to the wall, or to the central core plasma region (indicated by the large unnumbered central region in Fig. 1).

The interactions of the neutral atoms with the plasma are quite important just in front of the divertor plate, where the neutral atom density may be quite large (10^{20} to 10^{22} m^{-3}), and also in the edge of the confined central plasma region near the midplane, where the neutral atom density may be attenuated four to five orders of magnitude. The neutral atom density is also of some interest at the top of the plasma chamber, where the attenuation may be ten orders of magnitude or so, relative to the neutral atom density in the recycling region in front of the divertor plate.

As a further complication, the neutral atom transport problem in the edge of a fusion plasma is nonlinear because of the importance of neutral-neutral (atom-atom) scattering and because the "background" plasma medium in which the neutral transport is taking place depends on the neutral solution through atom-ion and atom-electron collisions. This nonlinearity is usually treated iteratively, which means that the neutral transport calculation must be made many times in converging the combined neutral-plasma solution.

*E-mail: weston.stacey@me.gatech.edu

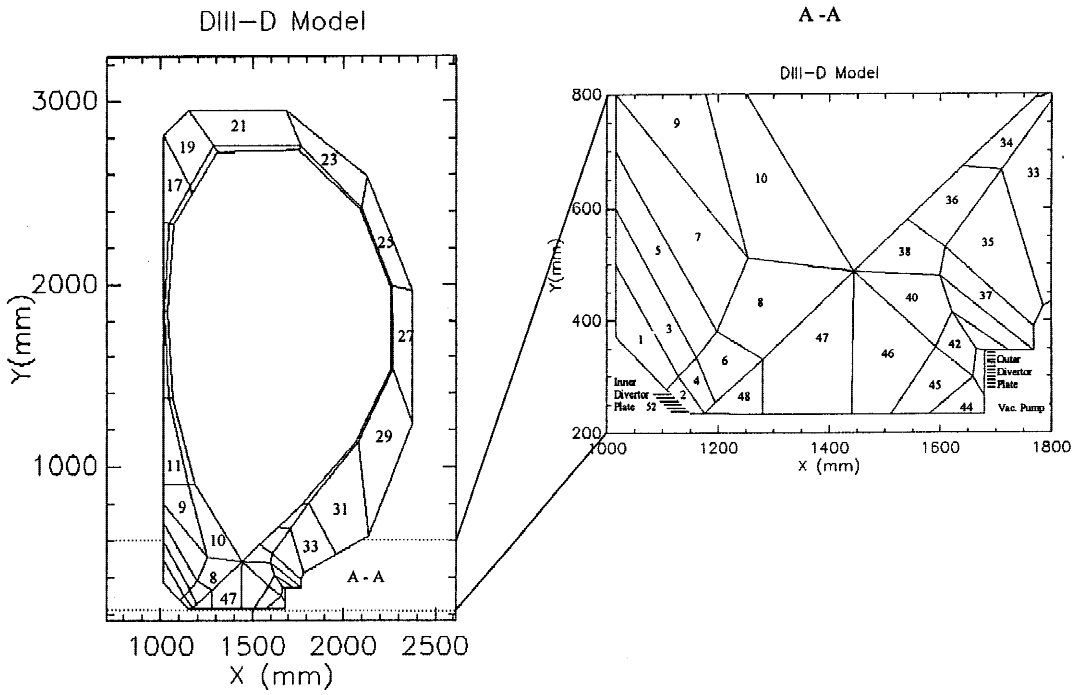

Fig. 1. Neutral atom transport model for the DIII-D plasma.

Neutral atom transport calculations in the edge of fusion plasmas are conventionally performed with Monte Carlo codes, in order to represent the geometrical complexity. However, when it is necessary to treat a large fraction of the edge plasma and to obtain accurate solutions throughout, Monte Carlo calculations can be quite time consuming (e.g., ~1 h to calculate the problem of Fig. 1). Moreover, because of its statistical nature, the Monte Carlo code is not well suited for an iterative plasma-neutrals solution.

In an effort to provide a practical neutral transport calculation that will enable the routine analysis of plasma-atomic reactions in the edge of fusion plasmas, we have proposed[1,2] what is essentially an interface current integral transport method. A number of approximations have been invoked in an effort to achieve computational efficiency: The collided component of the exiting current is calculated with escape probabilities using a rational approximation, and the fraction escaping across each surface is taken as proportional to the area of that surface; the transmission probabilities are calculated with a DP_0 angular distribution at every interface (i.e., the angular distributions within both the forward and backward half-spaces are assumed to be isotropic); the spatially distributed intraregion plasma temperature and density distribution is replaced by a uniform distribution with the same average mfp; etc. We have found that we can obtain acceptable accuracy at ~1% of the computational time of a Monte Carlo calculation, which makes the routine calculation of neutral-plasma reactions in the edge of fusion plasma experiments feasible.

We have now undertaken to isolate and check the accuracy of the various assumptions of our transport methodology by comparison with Monte Carlo and to construct correction factors or extend the methodology to improve the accuracy of the calculation when needed. The purpose of this paper is to report this work. Our basic interface current transport methodology is summarized in Secs. II and III. Then, the evaluation of the accuracy of various assumptions by comparison with Monte Carlo is discussed in Secs. IV through VIII.

II. INTERFACE CURRENT METHOD IN SLAB GEOMETRY

Subject to the assumption of angular fluxes at both boundaries, which are isotropic over the incident directional hemisphere (i.e., the DP_0 approximation), the assumption of a uniform spatial distribution of scattering sources within each mesh interval, and the assumption that neutrals emerge from scattering and charge-exchange events with an isotropic directional distribution, the interface current balance on a mesh interval Δ_i can be written[1]

$$\begin{bmatrix} J_i^+ \\ J_i^- \end{bmatrix} = \begin{bmatrix} (T_i^{-1}) & (-T_i^{-1}R_i) \\ (R_i T_i^{-1}) & (T_i - R_i T_i^{-1} R_i) \end{bmatrix} \begin{bmatrix} J_{i+1}^+ \\ J_{i+1}^- \end{bmatrix} + \frac{1}{2} s_i P_i \begin{bmatrix} -T_i^{-1} \\ 1 - R_i T_i^{-1} \end{bmatrix} , \quad (1)$$

where the total transmission probability T_i can be written as the sum of the first-flight transmission probability T_{0i} and the total reflection probability R_i:

$$T_i = T_{0i} + R_i = 2E_3(\Delta_i \Sigma_{ti}) + \tfrac{1}{2} c_i P_i (1 - 2E_3(\Delta_i \Sigma_{ti})) \ , \tag{2}$$

with E_3 being the exponential integral function and P_i being the total escape probability, which can be constructed from the first-flight escape probability P_{0i} for an isotropic collision rate distribution within the slab:

$$P_i = P_{0i} \sum_{n=0}^{\infty} [c_i(1 - P_{0i})]^n = \frac{P_{0i}}{1 - c_i(1 - P_{0i})} \ . \tag{3}$$

The first-flight escape probabilities are

$$P_{0i} = \frac{1}{\Delta_i \Sigma_{ti}} \left[\frac{1}{2} - E_3(\Delta_i \Sigma_{ti}) \right] , \tag{4}$$

and the number of secondary neutrals per collision is

$$c_i = \frac{\langle \sigma v \rangle_{scat} + \langle \sigma v \rangle_{cx}}{\langle \sigma v \rangle_{ion} + \langle \sigma v \rangle_{scat} + \langle \sigma v \rangle_{ex}} \ , \tag{5}$$

where the subscripts *ion*, *scat*, and *cx* refer to ionization, elastic scattering, and charge exchange, respectively, and the $\langle \sigma v \rangle$ are reaction rates averaged over the distributions of both species. The quantity s_i represents any external source of neutrals.

For boundary intervals adjacent to an isotropic plane source of neutrals, the inward first-flight transmission probability is

$$T_{0i} = E_2(\Delta_i \Sigma_{ti}) \ . \tag{6}$$

III. INTERFACE CURRENT METHOD IN TWO-DIMENSIONAL GEOMETRY

The interface current model in two dimensions can be written as follows:

$$J_{ij} = \sum_k^i T_{0i}^{kj} J_{ki} + \sum_k^i \left(1 - \sum_m^i T_{0i}^{km} \right) J_{ki} c_i \Lambda_{ij} P_i + s_i \Lambda_{ij} P_i \ . \tag{7}$$

Equation (7) states that the partial current from region i into region j, J_{ij}, is the sum of three contributions:

1. the fraction T_{0i}^{kj} of the partial currents incident on region i from region k, which are transmitted across region i without collision, summed over all regions k that are contiguous to i
2. the fraction of the incident partial currents that collided in region i times the probability c_i that the collision resulted in a secondary neutral times the probability $\Lambda_{ij} P_i$ that a neutral introduced uniformly and isotropically in region i escapes from region i into region j after zero or more subsequent collisions
3. the external source of neutrals introduced into region i times the probability that these source neutrals escape into region j. The total escape probability P_i is constructed from the first-flight escape probability P_{0i} by making use of Eq. (3).

With reference to Fig. 2, the first-flight partial current transmission coefficient across region i from region 1 to region 3 can be calculated for an angular flux distribution that is isotropic over the incident hemisphere of directions by considering the following:

1. the solid angle subtended by the exiting surface at a location ξ_1 on the incident surface
2. the average attenuation in an isotropic (over θ) distribution of path lengths between the incident and exit surfaces $\exp(-\Sigma R(\phi)) = \exp(-\Sigma l(\phi)/\cos\theta)$, where $\pi/2 \geq \theta \geq -\pi/2$ is the angle that the path length between incident and exiting surfaces makes with respect to the horizontal plane illustrated in Fig. 2
3. the definition of incident and exiting partial currents as integrals over the normal (to the surface) components of the (assumed) DP_0 angular flux distributions.

The resulting first-flight transmission probability from surface 1 to surface 3 is

$$T_{0i}^{13} = \frac{2 \displaystyle\int_{\xi_1^{min}}^{\xi_1^{max}} d\xi_1 \int_{\phi_{min}(\xi_1)}^{\phi_{max}(\xi_1)} d\phi \sin\phi_{out} K_{i_3}(\Sigma l(\phi(\xi_1)))}{(\xi_1^{max} - \xi_1^{min})} \ , \tag{8}$$

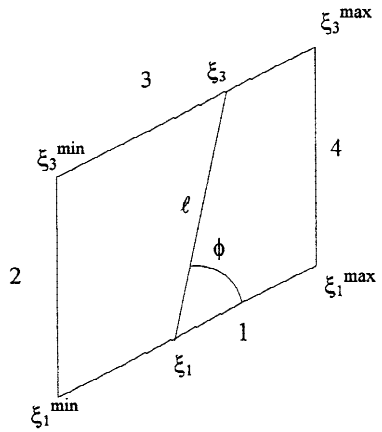

Fig. 2. Nomenclature for calculation of first-flight transmission probability.

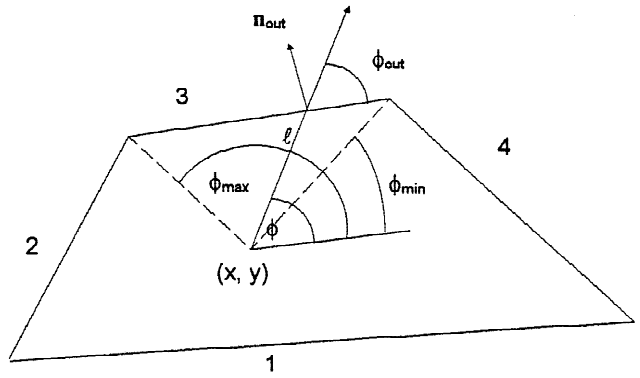

Fig. 3. Nomenclature for calculation of first-flight escape probability.

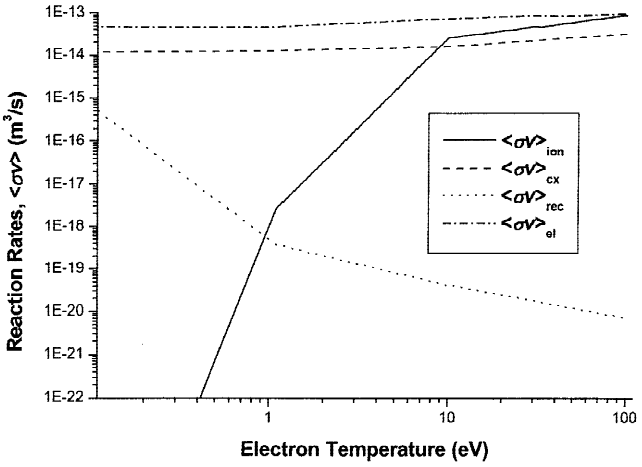

Fig. 4. Atom-electron ionization rate, ion-electron recombination rate, and atom-ion charge exchange and elastic-scattering rates.

where Ki_3 is the Bickley function of order $n = 3$. Analytical prescriptions have been developed[3] for the evaluation of this expression for regions of arbitrary shape bounded by straight-line segments or by arcs of circles.

Similar considerations for the attenuation of neutrals introduced isotropically at a point within region i in producing a current of uncollided neutrals into region 3, when averaged over a uniform collision or external source distribution in region i, lead to an expression for the first-flight escape probability from region i into region 3:

$$\Lambda_{i3} P_{0i} = \frac{1}{A_i} \int_{A_i} dxdy \int_{\phi \supset S_3} d\phi \sin \phi_{out} \frac{Ki_3(\Sigma l(\phi(x,y)))}{2\pi} , \tag{9}$$

where A_i is the planar cross section of region i. The limit $\phi \supset S_3$ on the integral over ϕ indicates the range of ϕ subtended by the interface with region 3 at the point (x, y) within region i, as illustrated in Fig. 3.

IV. FIRST-FLIGHT TRANSMISSION PROBABILITY

The calculation of transmission probabilities across uniform regions of various shapes using Eq. (8) have been compared with Monte Carlo calculations[4,5] and found to be in essentially exact agreement, confirming the reduction of the methodology to the computational algorithms and the coding.

The transmission probability depends on the optical thickness along the path followed from the entering to the exiting surfaces. If this optical thickness is calculated for all flight paths, then the first flight transmission probabilities can be calculated exactly. However, in the interest of computational efficiency, we do not want to calculate optical thickness along flight paths in nonuniform regions, but we would like to calculate an approximate optical thickness $(l/\langle\lambda\rangle)$ as the quotient of the length of the particular flight path l and an "average" mfp for the region $\langle\lambda\rangle$. Since $\lambda^{-1} \equiv \Sigma = N\sigma(T)$, using a linear average of $\langle N\rangle = 0.5(N_1 + N_2)$ is exact when the plasma density is linearly varying across a region, and it may be expected to be a reasonable approximation for other density variations. However, the variation in the ionization cross-section $\sigma_{ion}(T)$ does not vary linearly with temperature, although this is a more suitable approximation for the elastic scattering and charge-exchange rates, as illustrated in Fig. 4. Nevertheless, we try the simple approximation $\langle\lambda\rangle^{-1} = N\langle\sigma(T_{av})v\rangle/v_{av}$, with $T_{av} = 0.5(T_1 + T_2)$ and $v_{av} = [2m/T_{av}]^{1/2}$. Shown in Table I are the first-flight transmission probabilities for a slab in which the temperature varied linearly between the values at each boundary. For the smaller optical thickness, for which ~69% of the neutrals were transmitted without collision, the maximum error is 1.4%, resulting in an error of ~1% in the calculation. For the larger optical thickness, for which

TABLE I

$T_0 = 2E_3(l/\langle\lambda\rangle)$ for Slab with Linear Temperature Variation

	$T_1 - T_2$ (eV)			
	100 to 50	100 to 10	100 to 1	10 to 1
Optical thickness	2.130	2.252	2.244	2.164
T_0 exact	0.0513	0.0441	0.0446	0.0492
$T_0 = 2E_3(l/\langle\lambda\rangle)$	0.0517	0.0429	0.0410	0.0543
Optical thickness	0.213	0.225	0.224	0.216
T_0 Exact	0.689	0.676	0.677	0.685
$T_0 = 2E_3(l/\langle\lambda\rangle)$	0.690	0.673	0.669	0.694

only ~4 to 5% of the neutrals are transmitted without collision, the largest error of 10% occurs for the temperature range 10 to 1 eV over which the ionization rate varies dramatically with temperature; a 10% error in a 5% quantity is roughly a 0.5% error in the calculation. This level of accuracy is probably well within the uncertainty in the transmission coefficient associated with the estimated ±25% uncertainty in cross-section data. A 25% error in the cross section produces a 25% error in the optical thickness l_{op}, which translates into an $\approx[E_3(1.25l_{op})/E_3(l_{op}) - 1]$ error in transmission coefficient. For $l_{op} \approx 1$, this error is ≈28%. Furthermore, it has been found[6] that a 25% error in the cross section produces order unity uncertainties in the predicted neutral distributions and ionization rate distributions in neutral atom transport calculations in typical edge plasma models.

V. ESCAPE PROBABILITY

V.A. Test of Rational Approximation in Uniform Regions

In the interest of computational efficiency, we use a rational approximation for the first-flight escape probability of the form

$$P_0 = \frac{1}{x}\left(1 - \left(1 + \frac{x}{n}\right)^{-n}\right) , \qquad (10)$$

suggested by Wigner[7] ($n = 1$) and refined for cylinders by Sauer[8] ($n = 4.58$), where the parameter

$$x \equiv 4V/s\lambda \qquad (11)$$

is defined in terms of the surface area S, the volume V, and the mfp, instead of the more complex expression of Eq. (9). We note that Eq. (9) provides for the calculation of the particles escaping over each of the several segments of the surface bounding a region, whereas the rational approximation of Eq. (10) only provides for the calculation of the escape over the total bounding surface. In using this rational approximation, we must further define the probability Λ_{ij} that a neutral escaping from region "i" will escape over that segment of the surface taking it into contiguous region "j." We estimate the Λ_{ij} as the fraction of the bounding area (circumference) of region "i" that interfaces with region "j."

Our first test of the rational approximation was a series of Monte Carlo calculations[4,5] of the first-flight escape probability for a uniform distribution of neutrals in several uniform medium two-dimensional geometries with varying volume-to-surface ratios to determine if P_0 can be well characterized by the single parameter x of Eq. (11). As shown in Fig. 5, the first-flight escape probability is indeed well characterized by the parameter x.

We next investigated the accuracy of Eq. (10) as a function of the parameter n, for a variety of geometries and volume-to-surface ratios, again by comparison with Monte Carlo calculation of the first-flight escape probability for a uniform and isotropic neutral source distribution and uniform temperature and density. As is well known, Wigner's approximation ($n = 1$) underpredicts the escape probability for intermediate values of x. Sauer's theoretically motivated value $n = 4.58$ was confirmed as the best choice for circles (infinite cylinders). The best overall fit for all shapes was obtained with $n = 2.09$. A comparison of the rational approximation with $n = 1$, 2.09, and 4.58 is shown for a trapezoidal region in Fig. 6; the results were similar for other geometries, except the circle (cylinder), for which $n = 4.58$ was superior. The fit of Eq. (10) with $n = 2.09$ is compared with Monte Carlo results for various geometries in Fig. 7; except for the circle, the maximum error is 5% or less.

The fractional error in the total escape probability, $\epsilon = \Delta P/P$, is less than the fractional error in the first-flight escape probability, $\epsilon_0 = \Delta P_0/P_0$, as can be seen from using Eq. (3) to obtain

$$\epsilon = \epsilon_0\left[1 - \frac{cP_0}{1 - cP_0}\right] . \qquad (12)$$

Thus, use of Eq. (10) with $n = 2.09$ ($n = 4.58$ for circles) predicts the escape probability to within a few percent, which is sufficient accuracy given the ±25% uncertainty in the cross-section data.

V.B. Nonuniform Source Distribution

The escape probability formalism was developed initially from considerations of the escape of neutrals (neutrons actually) from a region over which a source was uniformly distributed. However, in front of the divertor plate, where a strong source of recycling neutrals is rapidly attenuated, the first collision source will be strongly peaked toward the source of recycling neutrals—the divertor plate. The first-flight and multiple-collision escape probabilities were calculated by Monte Carlo[4,5] for the source distribution shown in Fig. 8 by setting the number of secondary neutrals per collision to $c = 0$ and $c = 0.8$, respectively. The calculation was repeated for different values of the plasma density to obtain different values for the mfp. The results shown in Table II clearly demonstrate that the rational approximation yields quite accurate values for the escape probability (error <2%) except for the total escape probability in the situation when the dimension of the region is large compared to the mfp, for which the error is >5%.

V.C. Nonuniform Medium

Next, we consider the situation in which the source is uniform over the region, but the plasma density or temperature varies across the region. We consider very large variations in order to place an upper bound on the

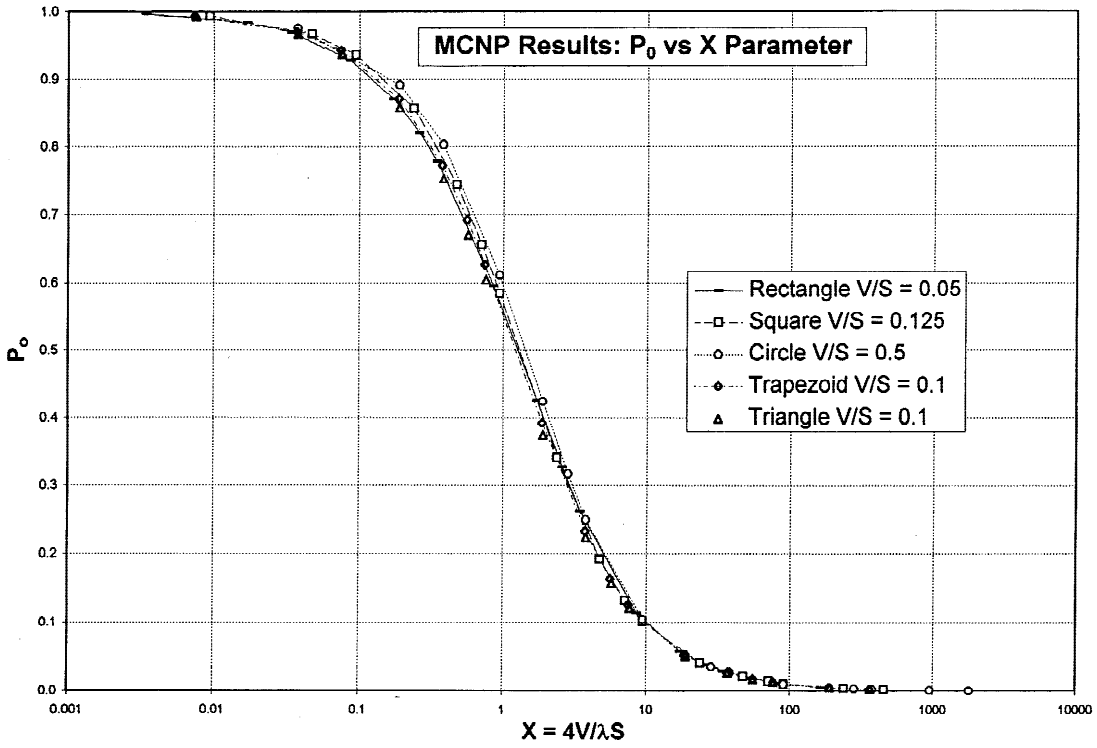

Fig. 5. First-flight escape probability as calculated by the Monte Carlo code for various geometries and surface-to-volume ratios plotted versus the parameter $x = 4V/S\lambda$.

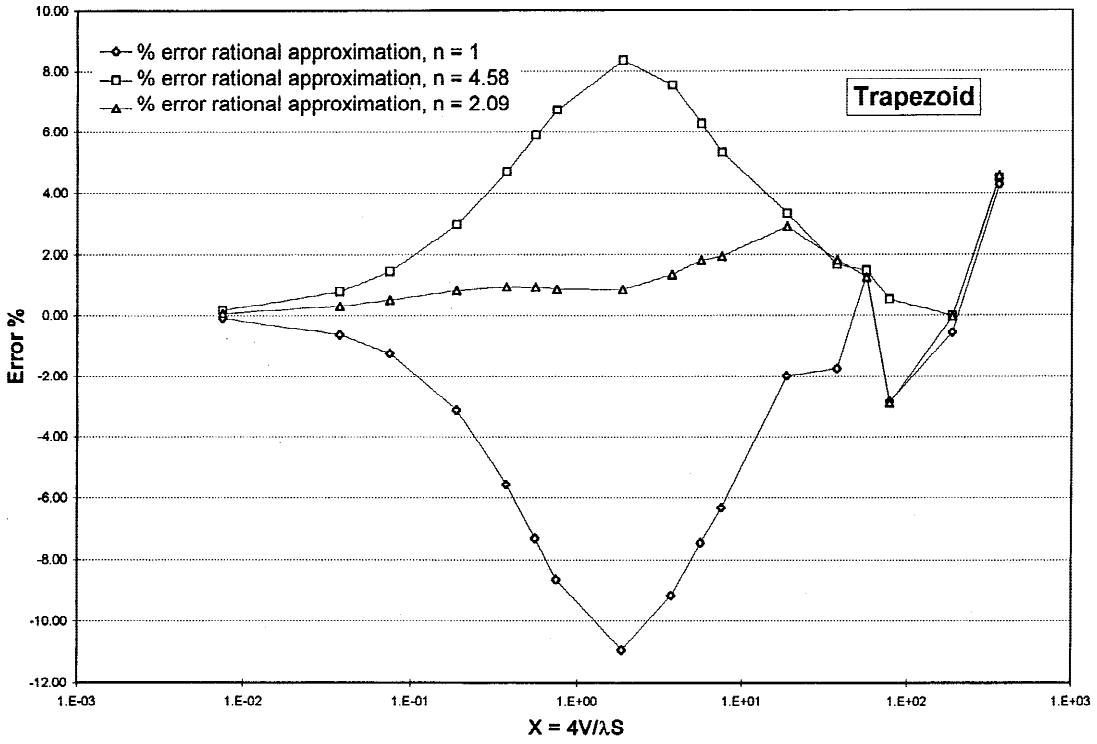

Fig. 6. Error in the different rational approximations for a trapezoidal region with volume-to-surface ratio 0.1.

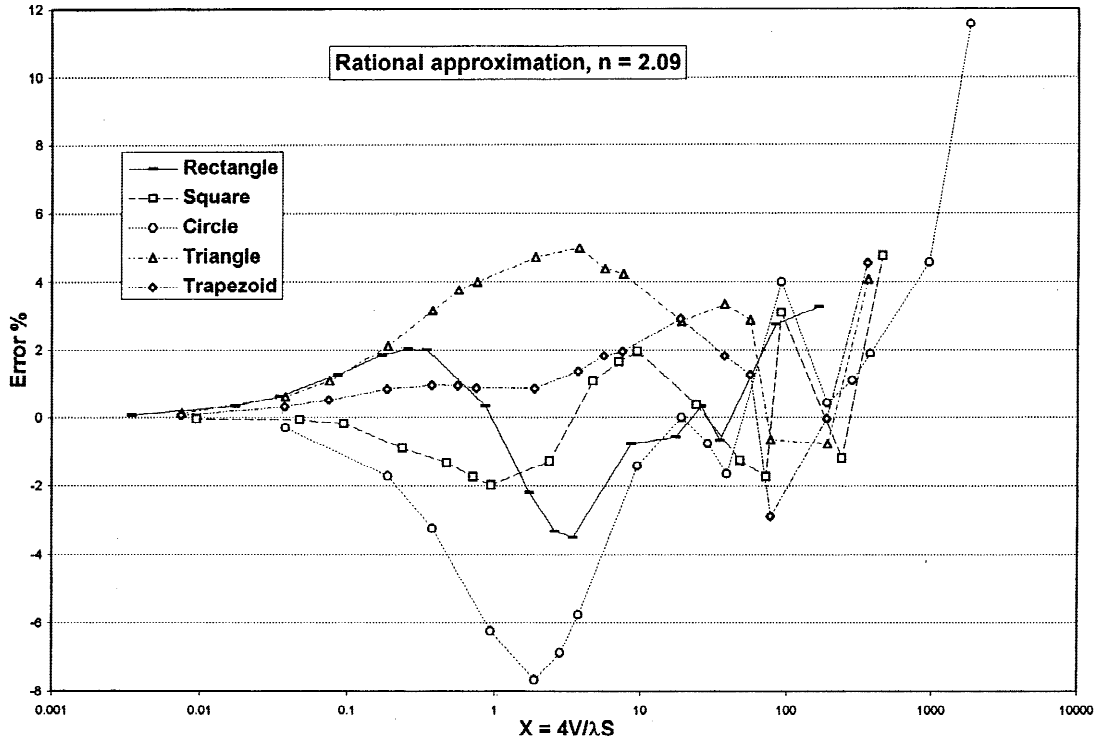

Fig. 7. Error in the new rational approximation ($n = 2.09$) for a variety of geometries.

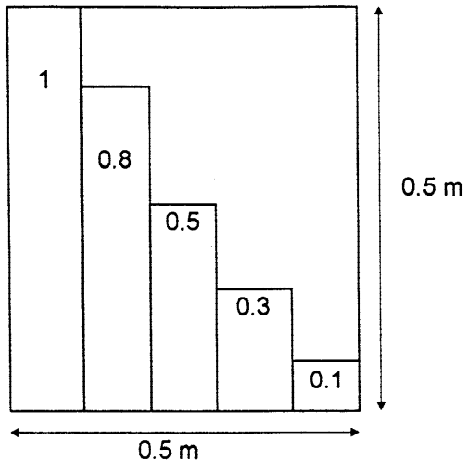

Fig. 8. Nonuniform source distribution for escape probability calculation.

TABLE II

Escape Probabilities for a Uniform (0.5- × 0.5-m) Square Medium with a Nonuniform Source Distribution

	mfp (m)		
	0.11	0.53	5.3
P_0 ($c = 0.0$) 1st flight			
Monte Carlo	0.194	0.587	0.938
Equation (10)	0.203	0.573	0.934
P ($c = 0.8$) total			
Monte Carlo	0.512	0.869	0.987
Equations (10) and (3)	0.548	0.865	0.985

effect. The effect of nonuniform density and temperature distributions within a region was investigated for a square region 0.5 m on a side. In the first set of calculations (shown in the first two columns of Table III), the density was uniform, but the temperature varied across the region from 100 eV on the left boundary to 10 or 1 eV on the right boundary. In the second set of calculations (shown in the last two columns of Table III), the temperature was uniform, but the density varied across the region from 1×10^{19} m^{-3} on the left boundary to 5×10^{18} and 5×10^{17} m^{-3} on the right boundary.

The escape probabilities were calculated exactly by Monte Carlo,[4,5] taking into account the variation in density or temperature. The escape probabilities were also evaluated using Eqs. (10) and (3) and linear averages of the density and temperature within the region to evaluate $\langle \lambda \rangle$. The calculations were made with the elastic scattering and charge-exchange cross sections set to zero to evaluate first-flight escape probabilities and again with

TABLE III

Escape Probabilities for Nonuniform Media

T (eV) n (m^{-3})	100 to 10 5×10^{18}	10 to 1 5×10^{18}	10 1×10^{19} to 5×10^{18}	10 1×10^{19} to 5×10^{17}
Optical thickness	0.903	0.174	0.706	0.494
P_0 ($\sigma_{cx} = \sigma_{el} = 0$)				
Monte Carlo	0.596	0.894	0.659	0.743
Eq. (10)	0.567	0.904	0.645	0.725
Optical thickness	2.25	2.16	3.35	2.35
P				
Monte Carlo	0.567	0.875	0.602	0.712
Eqs. (10) and (3)	0.553	0.895	0.623	0.708

the scattering and charge exchange cross sections nonzero to evaluate total escape probabilities. The results are shown in Table III. Using average values of plasma density and temperature to evaluate $\langle\lambda\rangle$ for use in the rational approximation of Eq. (10) provides estimates of P and P_0 that are accurate to within ~5% even when rather substantial plasma density and temperature variations occur over the region. This accuracy is adequate, given the uncertainty in the cross-section data.

V.D. Directional Escape Fractions with Nonuniform Source or Nonuniform Medium

We have established that Eqs. (10) and (3) provide an adequate prediction of the total escape probability across all surfaces from a region with a nonuniform source or nonuniform plasma temperature or density distribution. Now, we consider the effect of a nonuniform source or nonuniform plasma density or temperature on the fraction of escaping neutrals that escape across each surface; i.e., on the Λ_{ij} quantities. For a uniform source distribution and uniform plasma density and temperature, the fraction escaping across each surface is 0.25 for a square region. The results of the Monte Carlo calculation[4,5] of the directional escape fractions for the nonuniform source distribution illustrated in Fig. 8 are shown in Table IV. The nonuniform source causes a significant preferential escape across the surface nearest the peak in the source (the left surface in this case). The magnitude of this directional escape effect is inversely proportional to the mfp.

The effect of nonuniform density and temperature distributions within a region on the escape probability was investigated for a square region 0.5 m on a side. In the first set of calculations (shown in the first two columns of Table V), the density was uniform, but the temperature varied across the region from 100 eV on the left boundary to 10 or 1 eV on the right boundary. In the second set of calculations (shown in the last two columns of Table V), the temperature was uniform, but the density varied across the region from 1×10^{19} m^{-3} on the left boundary to to 5×10^{18} and 5×10^{17} m^{-3} on the right boundary.

TABLE IV

Directional Escape Fractions with Nonuniform Source

	mfp (m)		
	0.11	0.53	5.3
First flight ($c = 0.0$)			
Λ_{right}	0.073	0.154	0.195
Λ_{left}	0.431	0.348	0.307
Λ_{up}	0.247	0.250	0.249
Λ_{down}	0.250	0.249	0.250
Total ($c = 0.8$)			
Λ_{right}	0.109	0.168	0.196
Λ_{left}	0.393	0.332	0.305
Λ_{up}	0.248	0.249	0.249
Λ_{down}	0.250	0.250	0.250

The directional escape effect of a nonuniform temperature distribution is rather small. The directional escape effect of a factor of 20 density variation is significant, and we might be guided by the foregoing results to avoid creating calculational regions across which the plasma density would be expected to vary by more than about a factor of 5 to 10.

V.E. First-Flight Source Distribution Correction

A series of Monte Carlo calculations[4,5] were run for isotropic and cosine distributed sources incident on the left surface of a square region of dimension Δx, for a range of values of both Δx and mfp λ. The ratio of the number of neutrals escaping across the opposite (right)

TABLE V

Directional Escape Fractions with Nonuniform Medium

T (eV) n (m^{-3})	100 to 10 5×10^{18}	10 to 1 5×10^{18}	10 1×10^{19} to 5×10^{18}	10 1×10^{19} to 5×10^{17}
Optical thickness ($\sigma_{cx} = \sigma_{el} = 0$)	0.903	0.174	0.706	0.494
Λ_{right}	0.254	0.266	0.266	0.280
Λ_{left}	0.252	0.231	0.235	0.221
Λ_{up}	0.249	0.251	0.248	0.248
Λ_{down}	0.245	0.252	0.251	0.251
Optical thickness ($\sigma_{cx} \neq 0$, $\sigma_{el} \neq 0$)	2.25	2.16	3.35	2.35
Λ_{right}	0.247	0.263	0.280	0.313
Λ_{left}	0.256	0.234	0.223	0.195
Λ_{up}	0.248	0.251	0.248	0.244
Λ_{down}	0.249	0.252	0.249	0.248

forward (f) surface to the number escaping back (b) across the incident left surface, Λ_f/Λ_b, was fitted and is plotted as a function of $\Sigma\Delta x \equiv \Delta x/\lambda$ (the quantity $x = 4V/\lambda S = \Delta x/\lambda$ for a square) in Fig. 9, for several values of c_i. This ratio may be used to compute directional escape probabilities.

We note that the investigations of this and the previous three sections have been based on only a single

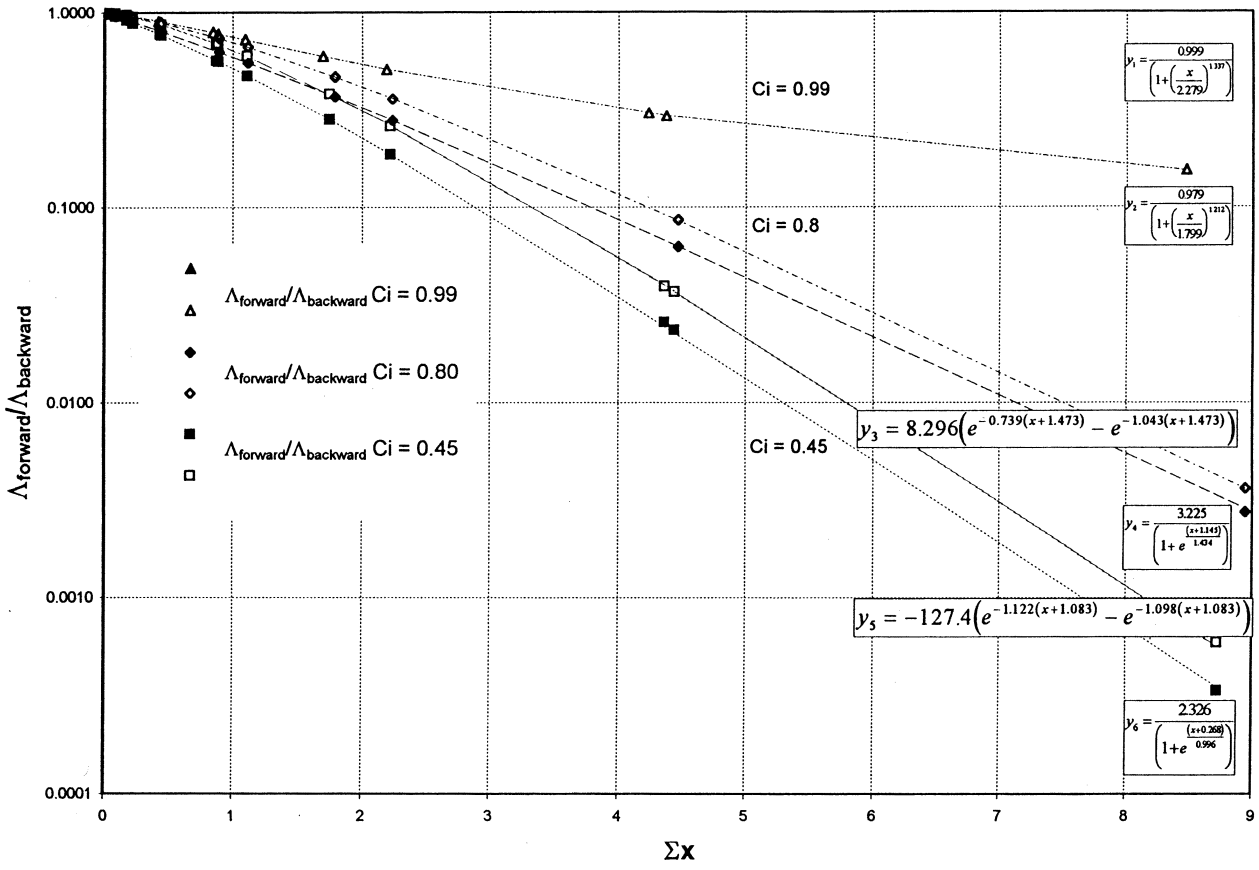

Fig. 9. Directional escape probability factor.

geometry—the square—and hence the results must be considered as indicative, rather than conclusive.

VI. ISOTROPIZATION OF THE ANGULAR DISTRIBUTION OF THE UNCOLLIDED FLUX AT INTERFACES

As presently formulated, the uncollided and collided neutral currents exiting a region are combined to obtain the neutral current entering the next region. The same angular flux distribution (isotropic in the incident hemisphere—DP_0) is assumed at each successive interface, for the purpose of calculating first-flight transmission probabilities. Since the angular distribution of those neutrals that penetrate several regions without collision will become progressively more forward directed, this isotropization approximation should break down for problems in which there is a large component of uncollided neutrals that penetrate several regions. This point is made clear by considering the limiting case $\sigma_{cx} = \sigma_{el} = 0$ (i.e., $c = 0$) in which neutrals are only ionized (removed). In this case, the transmitted current at a distance L from a plane with an incident isotropic angular distribution of neutrals constituting a current J_0 is exactly $J(L) = J_0 2E_3(L/\lambda)$. If the interval L is subdivided into N equally spaced subintervals, the current at L that would be calculated by the interface current method is

$$J'(L)/J_0 = \prod_{n=1}^{N} 2E_3(L/N\lambda) \neq 2E_3\left(\sum_{n=1}^{N}\left(\frac{L}{N}\right)\Big/\lambda\right) = 2E_3(L/\lambda) \ . \quad (13)$$

To evaluate the magnitude of this effect, we consider a slab with $\sigma_{cx} = \sigma_{el} = 0$ (i.e., $c = 0$) and optical thickness 5 with a plane isotropic source incident on the left boundary. (Note that with a plane isotropic source, the exact solution at a distance L is $J(L) = E_2(L/\lambda)J(0)$, but the same problem persists.) The Monte Carlo calculation[4,5] and several interface current calculations, each corresponding to dividing the slab into different computational subdivisions, are shown in Fig. 10. (The parameter x in Figs. 10 and 11 is the linear dimension.) When the subdivisions are less than about one-half mfp, the present calculation procedure of isotropizing the angular flux distribution at interfaces, for the purpose of calculating transmission probabilities, introduces a substantial error in the calculation of the penetration of the uncollided flux component.

It is possible, in principle, to make a separate calculation of the collided and uncollided components of the neutral flux in order to avoid this problem. However, it seems that the problem can also be avoided by choosing calculational regions that are at least one-half mfp thick (which could cause a problem if the method was used to calculate detailed neutral distributions on a fraction of an mfp scale length) or by applying a correction factor as discussed in Sec. VII. It is also possible, of course, to formulate the calculation with a higher order DP_n expansion of the angular flux distribution and calculate directly the increasing anisotropy, but we are interested in obtaining a computationally economical model.

VII. PENETRATION PROBLEMS

The foregoing discussion suggests that there might be difficulty in calculating penetration problems because of the isotropization assumption and because of the failure to account for the directionality of the escape probability. The presence of charge exchange and elastic scattering, which combined have a reaction rate typically about four times the ionization rate, should substantially reduce the error caused by the isotropization assumption. The error caused by the escape probability directionality problem can be fixed by using the directional escape probability correction factor from Fig. 9. Defining forward f and backward b reflection coefficients

$$R_i^{f/b} \equiv \Lambda_{f/b}^i \frac{c_i P_{0i}[1 - 2E_3(\Delta_i \Sigma_{ti})]}{1 - c_i(1 - P_{0i})} \ , \quad (14)$$

where

$$\Lambda_f^i \equiv \frac{1}{1 + (\Lambda_f/\Lambda_b)_i^{-1}} \ , \quad \Lambda_b^i \equiv \frac{1}{1 + (\Lambda_f/\Lambda_b)_i} \quad (15)$$

incorporates the directionality correction (Λ_f/Λ_b) plotted in Fig. 9; the transmission and reflection coefficients in Eq. (1) are replaced by $T_i \rightarrow T_{0i} + R_i^f$ and $R_i \rightarrow R_i^b$.

As a test case, a uniform slab model of thickness 10 mfp was calculated. The Monte Carlo result is shown as the solid line in Fig. 11, and the interface current results without any correction factor are shown as solid symbols. Four different interface current calculations were made, breaking the slab into regions of 0.45, 0.98, 2.2, and 4.45 mfp thickness. The uncorrected interface current results have two compensating errors, as discussed earlier:

1. Equal forward and backward escape probabilities are assumed $(\Lambda_f = \Lambda_b)$, which causes forward penetration to be overpredicted.

2. The anisotropic uncollided component of the current is isotropized at every region interface, which causes forward penetration to be underpredicted.

Note that the escape directionality error 1 is dominant for subdivision into regions of thickness greater than 1 mfp, the isotropization error 2 is dominant for subdivision into regions of thickness <1 mfp, and the two errors almost exactly compensate for regions of thickness

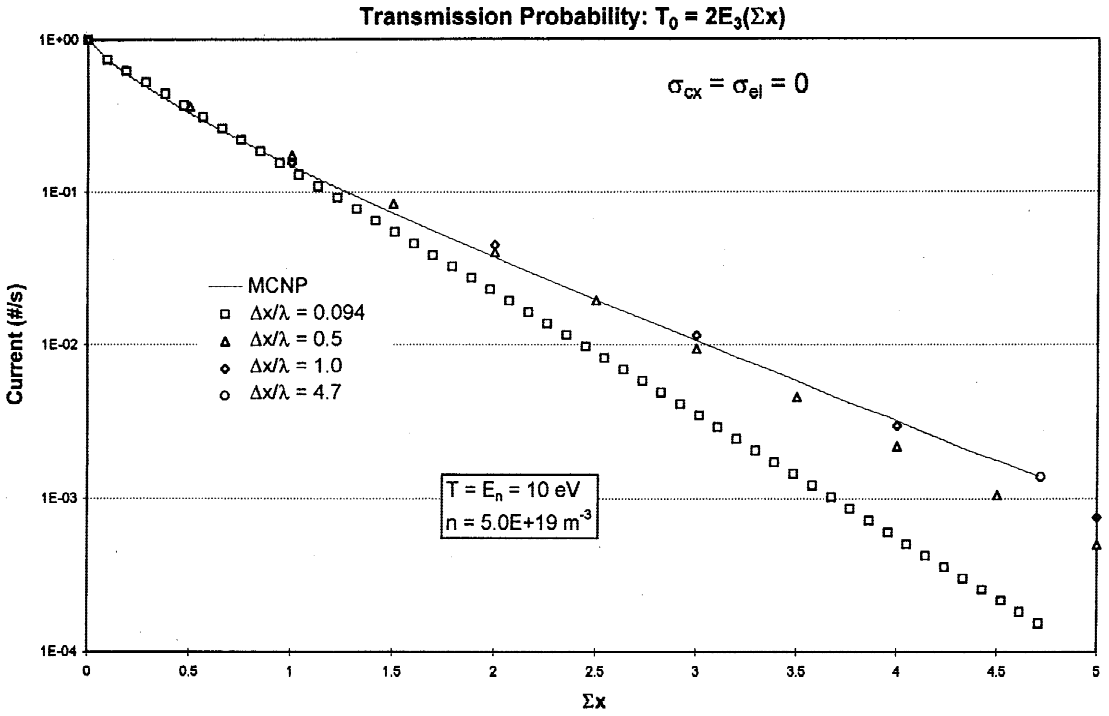

Fig. 10. Effect of isotropizing uncollided flux at interfaces.

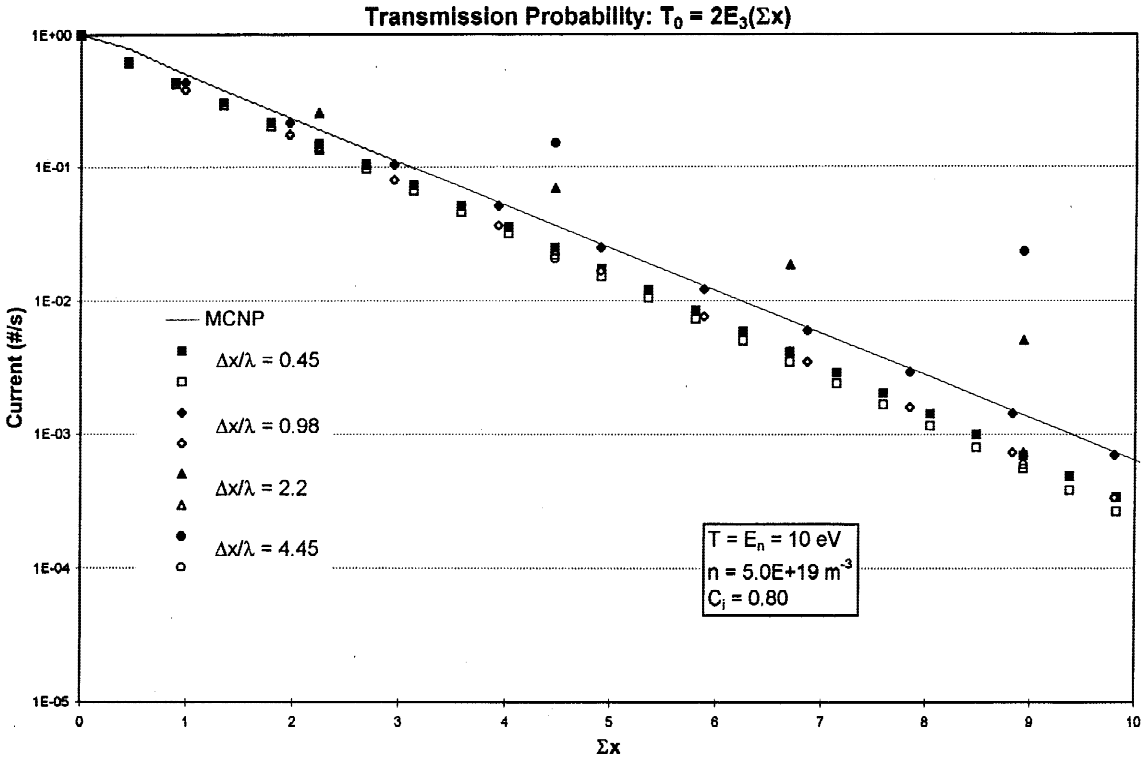

Fig. 11. Penetration of an incident current (closed symbols uncorrected, open symbols corrected).

TABLE VI

Effective Transmission and Reflection Probabilities*

$\frac{\Delta x}{\lambda} = n$	$\hat{T}_i$	$\hat{R}_i^b$
$\frac{1}{2}$	$\left[T_i\left(1-\left(\frac{\frac{1}{2}c_iP_i}{1+T_i}\right)^2\right)\right]^{1/2}$	$\frac{\frac{1}{2}c_iP_i}{1+T_i}$
2	$\frac{T_i^2}{(1-(\frac{1}{2}c_iP_i)^2)}$	$\frac{1}{2}c_iP_i\left[1+\frac{T_i^2}{(1-(\frac{1}{2}c_iP_i)^2)}\right]$
3	$\frac{T_i^3}{(1-(\frac{1}{2}c_iP_i)^2)^2-(\frac{1}{2}c_iP_i)^2T_i^2}$	$\frac{1}{2}c_iP_i\left[\frac{1+T_i^2(1-(\frac{1}{2}c_iP_i)^2)+T_i^4}{(1-(\frac{1}{2}c_iP_i)^2)^2-(\frac{1}{2}c_iP_i)^2T_i^2}\right]$

*For regions with $\Delta/\lambda = n = \ldots \frac{1}{3}, \frac{1}{2}, 1, 2, 3 \ldots (T_i = T_i(\Delta x/\lambda = 1) = T_i^o(\Delta x/\lambda = 1) + \frac{1}{2}c_iP_i(1 - T_i^o)$, $\hat{R}_i^f = c_iP_i(1 - T_i^o) - \hat{R}_i^b$, $\hat{T}_i^o = \hat{T}_i - \hat{R}_i^f$, $\bar{P}_i = P_i(1)(1 - T_i^o(1)))$.

$\sim$1 mfp; this result is approximately independent of the value of c_i.

When the directional escape probability factors Λ_{fb} are used, the first error is corrected, and the four different interface current calculations (3, 5, and 20 regions) yield essentially the same result (indicated by the empty symbols in Fig. 11), all underpredicting the correct (Monte Carlo) penetration because of the second (interface isotropization) error.

The fact that the isotropization and escape directionality errors almost exactly cancel for $\Delta x/\lambda = 1$ allows effective transmission and reflection probabilities to be

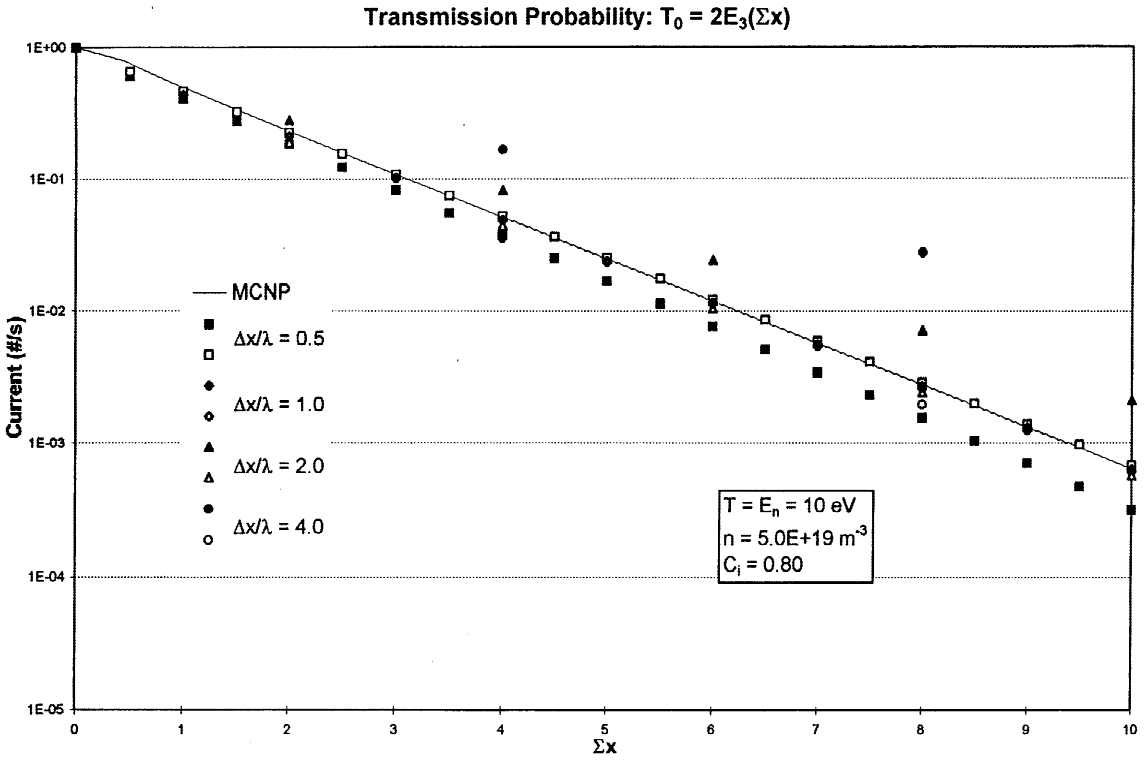

Fig. 12. Penetration of an incident current with effective transmission and reflection probabilities (closed symbols uncorrected, open symbols with effective probabilities).

constructed for regions with $\Delta x/\lambda = n = \frac{1}{3}, \frac{1}{2}, 1,2,3,\ldots$ by solving

$$\kappa\left(\frac{\Delta x}{\lambda} = n\right) = \left[\kappa\left(\frac{\Delta x}{\lambda} = 1\right)\right]^n ,$$

where κ is the matrix on the right side of Eq. (1). The resulting transmission and reflection probabilities are shown in Table VI for the first few values on n. "Non-integral" values of n or $1/n$ would be treated by interpolation between integral values to obtain effective transmission and reflection coefficients.

These effective transmission and reflection probabilities were used to solve the same penetration problem as discussed earlier for Fig. 10. As can be seen from Fig. 12, use of the effective probabilities of Table VI results in a significant improvement in deep penetration problems relative to the use of the uncorrected transmission and escape probabilities of Eqs. (2), (3), and (4) with $\Lambda_f/\Lambda_b = 1$.

VIII. SUMMARY AND CONCLUSIONS

An interface current method has been formulated for the transport of neutral atoms in the geometrically complex edge region of a fusion plasma. The individual approximations of the transport method have been isolated and tested by comparison with Monte Carlo calculations, and correction factors and extensions of the methodology have been developed as necessary to improve accuracy. Several results that may be useful in other applications of interface current methods have been developed:

1. a Sauer-type rational approximation for noncylindrical geometries
2. directional "first-flight" corrections for escape probabilities
3. improved transmission and escape probability definitions.

Having validated the basic transmission/escape probability (TEP) transport methodology and evaluated the accuracy/limitations imposed by a number of assumptions made in its practical implementation, we are now undertaking a series of TEP/Monte Carlo comparison calculations for several realistic experimental models, including a set of experiments in which the neutral density was measured in the plasma edge. These calculations will provide a practical evaluation of the TEP method for realistic models and will be published in future papers.

REFERENCES

1. W. M. STACEY, *Phys. Plasmas*, **4**, 179 (1997).

2. W. M. STACEY and J. MANDREKAS, *Nucl. Fusion*, **34**, 1385 (1994).

3. R. RUBILAR, "Neutral Particle Transport in the Plasma Edge and Divertor Region," PhD Thesis, Georgia Institute of Technology.

4. "MCNP—A General Monte Carlo *N*-Particle Transport Code. Version 4B," Los Alamos LA-12625, Los Alamos National Laboratory (1997).

5. D. B. HEIFETZ, D. POST, M. PETRAVIC, J. WEISHEIT, and G. BATEMAN, *J. Comput. Phys.*, **46**, 309 (1982).

6. W. M. STACEY, E. W. THOMAS, and T. M. EVANS, *Phys. Plasmas*, **2**, 3740 (1995).

7. E. P. WIGNER et al., *J. Appl. Phys.*, **2**, 257 (1955).

8. A. SAUER, "Approximate Escape Probabilities," *Nucl. Sci. Eng.*, **16**, 329 (1963).

Weston M. Stacey (BS, physics, 1959, and MS, nuclear science, 1963, Georgia Institute of Technology; PhD, nuclear engineering, Massachusetts Institute of Technology, 1966) is the Callaway Regents' Professor of Nuclear Engineering at Georgia Institute of Technology. His current research interests include tokamak plasma edge physics and fusion reactor conceptual design.

John Mandrekas (PhD, University of Illinois, 1987) is a senior research scientist at the Georgia Institute of Technology Fusion Research Center. His research interests are in computational plasma physics, neutral transport theory, and the analysis of plasma physics experiments.

Roberto Rubilar (PhD, Georgia Institute of Technology, 2000) recently completed his PhD thesis and is now employed as a nuclear engineer at the Knolls Atomic Power Laboratory.